frontiers | Frontiers in Energy Research

TYPE Original Research
PUBLISHED 11 July 2024
DOI 10.3389/fenrg.2024.1422256

OPEN ACCESS

EDITED BY
Abdolali K. Sadaghiani,
Sabancı University, Türkiye

REVIEWED BY
Bittagopal Mondal,
Council of Scientific and Industrial Research (CSIR), India
Yacine Addad,
Khalifa University, United Arab Emirates

*CORRESPONDENCE
Suvash C. Saha,
Suvash.Saha@uts.edu.au

RECEIVED 23 April 2024
ACCEPTED 17 June 2024
PUBLISHED 11 July 2024

CITATION
Al-Waaly AAY, Tumpa SA, Nag P, Paul AR, Saha G and Saha SC (2024), Entropy generation associated with natural convection within a triangular porous cavity containing equidistant cold domains.
Front. Energy Res. 12:1422256.
doi: 10.3389/fenrg.2024.1422256

Entropy generation associated with natural convection within a triangular porous cavity containing equidistant cold domains

Ahmed A. Y. Al-Waaly[1], Sadia Alam Tumpa[2,3], Preetom Nag[2,3], Akshoy Ranjan Paul[4], Goutam Saha[5] and Suvash C. Saha[6]*

[1]Department of Mechanical Engineering, College of Engineering, Wasit University, Kut, Iraq, [2]Department of Mathematics and Physics, North South University (NSU), Dhaka, Bangladesh, [3]Center for Applied and Computational Sciences (CACS), North South University (NSU), Dhaka, Bangladesh, [4]Department of Applied Mechanics, Motilal Nehru National Institute of Technology Allahabad, Allahabad, India, [5]Department of Mathematics, University of Dhaka, Dhaka, Bangladesh, [6]School of Mechanical and Mechatronic Engineering, University of Technology Sydney, Sydney, NSW, Australia

This study investigates the computational analysis of steady, incompressible, natural convection airflow in a 2D equilateral triangular cavity featuring two stationary cold circular cylinders. The convective phenomena within the cavity have been observed under the variation of uniform porosity. The convective flow has been modeled using the Darcy-Brinkman formulations for porous medium incorporated with the Boussinesq approximation. The governing equations have been simulated using the finite element method with non-uniform triangular meshing. The investigation was conducted with a fixed Prandtl number, Pr = 0.71, and different porosity by varying Darcy number, $Da = 10^{-5}$ to 10^{-2}. The convective strength has been varied with the Rayleigh number, $Ra = 10^3$ to 10^6, and the length of the heated and cold segment, $\varepsilon = 0.1$ to 0.9. Results regarding the fluid flow and temperature distribution are visualized through streamlines and isotherms. The quantity and the quality of heat transfer (HT) have been investigated, respectively, by the Nusselt number (*Nu*) and the entropy generation (E_{gen}). The results reveal that an increase in the length of the hot wall (ε) significantly reduces HT. Also, E_{gen} increases with the length of active segments (ε), while the Bejan number (*Be*) consistently rises when the Darcy-Rayleigh (*Da*-*Ra*) number increases, i.e., $Da\text{-}Ra \geq 10^2$. The maximum HT rate was obtained within the range of $Da = 10^{-5}$ to 10^{-3} for a constant value of ε. Furthermore, the maximum HT was obtained for the smallest value ε for any value of *Da* or *Ra*.

KEYWORDS

triangular cavity, heat transfer, entropy generation, nusselt number, bejan number

1 Introduction

Natural convection (NC), induced by buoyancy forces arising from temperature differences, is readily observed in nature (Bhowmick et al., 2019). It represents a fundamental heat transfer (HT) phenomenon occurring across various geometries, crucial for regulating temperatures within enclosed spaces. Understanding NC is essential for optimizing HT processes in different engineering industries, as it connects

passive mechanisms, thereby reducing energy consumption and environmental impact (Liu et al., 2019). The various shapes of cavities influence NC by modifying fluid dynamics and HT behavior, leading to optimized thermal efficiency in heat exchangers and enhanced cooling in electronic devices, underscoring the significance of cavity design in engineering applications. NC in V-shaped cavities transitions from conduction at low Rayleigh number (*Ra*) to asymmetry at moderate *Ra* and chaos at high *Ra* (Bhowmick et al., 2019). Furthermore, valley-shaped cavities exhibit two flow phases affected by aspect ratios and *Ra*, allowing for the prediction of stratification breakup times and Nusselt number (*Nu*) trends, highlighting the importance of validating field measurements (Bhowmick et al., 2018). Among all cavity shapes, triangular cavities play a crucial role due to their ability to induce complex flow patterns, providing insights into fundamental fluid dynamics and HT phenomena. These cavities are extensively used in designing aircraft wings, heat exchangers, microfluidic devices, rocket nozzles, and various other applications, including heating and cooling (Sharif and Mohammad, 2005). Triangular cavities enhance turbulence, thereby boosting HT efficiency, as evidenced by studies on heater placement demonstrating *Nu* (Das et al., 2017). Additionally, HT in isosceles triangular geometries is influenced by various factors, with smaller nanoparticles enhancing HT and larger ones causing stagnation (Uddin et al., 2022). A computational study on a zigzag-bottom triangular cavity reveals disrupted symmetric fields with higher Lewis numbers (*Le*), enhanced HT and mass transfer (MT) at positive buoyancy ratios, and higher *Ra* values. Furthermore, it uncovers a surprising dominance of conduction over convection at higher *Ra* values with negative buoyancy ratios, providing insights into the role of buoyancy in MT and HT (Rahman et al., 2012).

Exploring HT in triangular chambers filled with nanofluid reveals complex interactions between buoyancy, *Ra*, *Le*, and buoyancy ratio parameters (Sheremet et al., 2017). This understanding is crucial as it unveils three intervals in the average Nusselt number (Nu_{avg}), shedding light on nanofluid (NF) dynamics and critical factors affecting MT and HT. Similarly, investigations into HT and fluid flow in undulated triangular hollows showcase dominant HT, highlighting a complex interaction between parameters and geometry in triangle cavities (Bhardwaj and Dalal, 2013). Additionally, studies on magnetohydrodynamics (MHD) NC in triangular solar collectors confirm that HT improves with higher *Ra* values while conduction HT dominates at lower *Ra* values. Adjusting nanoparticle diameter offers insights for optimizing HT efficiency (Rahman et al., 2016). Furthermore, exploring flexible-sided triangular cavities with MHD reveals varied HT effects, providing insights into the intricacies of fluid dynamics and HT (Selimefendigil and Öztop, 2016). Examining radiative and natural convection HT in inclined triangle cavities with nanofluid and magnetic fields indicates increased HT and total E_{gen} for higher *Ra* values and lower Hartmann number (*Ha*) (Afrand et al., 2020). Likewise, two-phase NC studies in triangular geometries with wavy hot walls and magnetic fields exhibit complex effects of parameters, offering insights for system optimization (Shekaramiz et al., 2021).

Another area of interest in convective HT study deals with mixed convection (MC), involving both buoyancy-driven and externally-driven forced convection (FC) within a fluid flow and HT system. Numerical simulations in triangular cavities with oscillating lids detect transitions to locked-on flows with repeated HT rate fluctuations. This reveals an increase in Nu_{avg} with the dimensionless frequency of lid velocity (Chen and Cheng, 2009). Moreover, investigations into mixed convection HT in triangular cavities underscore the impact of external factors like magnetic fields and Reynolds number (*Re*) on *Nu* (Soomro et al., 2020). In triangular cavities with nanofluid and internal heating, MC leads to *Nu* deterioration with increased Richardson number (*Ri*), highlighting the role of nanoparticle introduction during negative *x*-direction wall movement for enhancing HT (Selimefendigil and Öztop, 2017). Furthermore, the direction of motion of sliding walls plays a crucial role in controlling temperature and flow fields, maximizing HT in lid-driven cavity flows (Hasanuzzaman et al., 2012). Finally, MC in nanofluid-filled triangular cavities demonstrates enhanced HT influenced by nanoparticle concentrations and *Ri*, emphasizing the efficiency of solid volume fraction as a control parameter (Rahman et al., 2011).

Examining water based alumina oxide NF within a lid-driven triangular cavity unveils distinct variations in HT rates across different electrical conductivity models, and *Nu* decreased with the increase of *Ri* and *Ha* values (Chamkha et al., 2018). Furthermore, computational analysis of MT and mixed convection HT within a lid-driven right-angled triangular cavity exposes a notable influence of buoyancy ratio and lid movement direction on heat and mass transfer under varying *Ri* (Ching et al., 2012). Also, analysis using finite element method (FEM) on Cu-H_2O nanofluid within inclined triangular cavities illustrates an augmented HT with higher nanoparticle concentration, affirming the significant impact of solid volume fraction on thermal fields and flow patterns. It identifies the Grashof number (*Gr*) and solid volume percentage as pivotal control parameters (Billah et al., 2013). Additionally, a study delves into a viscous fluid in a triangular cavity with a central square obstacle, revealing amplified kinetic energy and convective HT coefficients with increased *Ra*. Addressing singularity issues through non-uniform heating provides crucial insights into fluid dynamics and thermal behavior in such configurations (Bilal et al., 2020). Moreover, investigating corner-heated triangular cavities with magneto-NF underscores the substantial influence of *Ra* and cavity orientation on thermo-fluid flow structures and HT rates. Furthermore, escalating *Ha* compromises HT rates and flow velocity, whereas Al_2O_3-H_2O nanofluid consistently enhances HT properties (Nag et al., 2022). In addition, a numerical exploration of CuO-H_2O nanofluid within an isosceles triangular geometry demonstrates that a higher nanoparticle percentage enhances HT rates, while an increase in particle diameter restrains the rate of HT. A strong magnetic field diminishes fluid flow circulation and the intensity of HT rates (Uddin et al., 2022). Reversed trends in NF convection within an isosceles triangle are observed in response to changes in the magnetic field (Chatterjee et al., 2022).

Several investigations have explored the intriguing NC phenomenon within triangular cavities containing porous medium. One study investigated HT dynamics in a porous triangular cavity nestled between square tubes, spanning a wide range of parameters. It advocates for using fluids possessing higher Pr to optimize HT in the upper cavity, whereas the lower cavity

demonstrates consistent HT behaviors across different fluid types (Basak et al., 2010). Concurrently, scrutinizing various temperature boundary conditions, another study explores NC flow and HT in a porous triangular cavity. Placing a heater at the bottom wall causes multiple vortex formations, amplifying HT compared to alternative configurations (Varol et al., 2008a). Furthermore, a separate investigation explores NC flow and HT in non-isothermally heated porous triangular cavity, employing finite difference (FD) techniques and Darcy's law to gather insights into the complex dynamics (Varol et al., 2008b). These studies collectively deepen our understanding of NC within triangular cavities and underscore the significance of factors such as fluid properties, boundary conditions, and geometric configurations in governing HT phenomena.

Furthermore, E_{gen} within the cavity during flow and HT underscores the irreversible nature of these processes, attributed to viscous dissipation and temperature gradients. Thus, minimizing E_{gen} emerges as a critical aspect in enhancing the productivity of flow and HT systems. A numerical investigation delves into the effects of sinusoidal heating and a wavy wall on E_{gen} and HT within a porous right triangular cavity. The findings illustrate a transition from conduction dominance at low *Da* to intensified convection with undulated walls, resulting in a noteworthy 53% increase in the maximum *Nu* (Bhardwaj et al., 2015). Similarly, exploration of NC within a triangular cavity hosting a rectangular heat source reveals the occurrence of counter vortexes, heightened effectiveness at higher *Ra*, and complex HT patterns with varying heat source sizes. Unexpectedly, a proportional increase in temperature with heat source size yields a decrease in Nu_{avg}, particularly along the hot wall, highlighting optimal results at the smallest heat source size and a *Ra* of 10^6 (Fayz-Al-Asad et al., 2021). Additionally, examining E_{gen} within right-angled triangle cavities containing porous media identifies specific locations experiencing maximum E_{gen}, with overall entropy augmentation corresponding to increasing *Da*. Also, triangular cavities featuring a 15° top angle demonstrate superior HT rates, enhanced thermal mixing, and diminished total E_{gen} across diverse fluid processing scenarios (Basak et al., 2012). Moreover, the study of NC of non-Newtonian fluid within a magnetic field in triangular cavities shows complex dynamics affecting HT, *Nu*, E_{gen}, and transmission rates (Li et al., 2020). Some recent research in cavities is also found in (Amidu et al., 2021; Ikram et al., 2021; Kumar et al., 2021; Riahi et al., 2022; Ikram et al., 2023; Kumar et al., 2023; Saboj et al., 2023; Saha et al., 2023; Saha B. K. et al., 2024; Saha G. et al., 2024; Saha T. et al., 2024; Ikram et al., 2024; Saboj et al., 2024).

Drawing from the literature review provided above, the examination of HT and E_{gen} within a triangular cavity holds significance for enhancing the performance of various systems, including cooling mechanisms, heat exchangers, and fluid flow systems. To the authors' knowledge, there has yet to be any prior exploration into the equilateral triangular cavity scenario featuring constant heat applied on the bottom wall segment coupled with the insertion of two circular cold objects within the cavity. Consequently, this study aims to investigate fluid flow, HT, and porous medium characteristics within such a triangular cavity employing air as the base fluid. The study will assess the impact of *Ra*, *Da*, and the size of the length of the applied heat flux on E_{gen}, fluid flow, and HT behavior. Specifically, the investigation will focus on parameters such as the average *Nu*, *Be*, streamlines and isotherms presentation, and E_{gen} of fluid flow and HT.

In brief, the model's findings can enhance the design of eco-friendly cooling systems for buildings, cutting energy usage and tackling urban heat islands in hot climates. In buildings, especially in regions with hot/cold climates, effective cooling/heating is crucial in upholding comfortable indoor temperatures while minimizing energy usage. Passive cooling systems utilize natural phenomena, such as convection and radiation, to remove heat from the building without relying heavily on mechanical cooling systems like air conditioners. Porous cavities are often integrated into building designs to facilitate NC and heat dissipation. The model investigated could be used to study E_{gen} associated with NC within porous cavities, such as those integrated into building designs (Mansouri et al., 2022; Li et al., 2023). By understanding how E_{gen} influences HT and energy efficiency, engineers and architects can optimize the design of these passive cooling systems to enhance their performance and reduce energy consumption.

Moreover, the study investigates NC in a triangular porous cavity with cold domains, focusing on E_{gen} and HT. It has practical applications in engineering, environmental sciences, and energy systems. Insights from the study can improve cooling systems for electronics, heat exchangers, building features for natural airflow, greenhouse ventilation, filtration systems, solar collectors, and industrial drying chambers. By optimizing the design and geometry of these systems, efficiency and performance can be significantly enhanced, leading to better heat distribution, energy savings, and improved process outcomes.

2 Physical model and governing equations

The present research investigates NC within a 2D porous triangular cavity featuring two stationary cold cylinders. The study explores the behavior of different fluids (air and water). Each side of the triangular cavity is assumed to have a length of L, as depicted in Figure 1. The segment of inclined walls, along with the two cylinders, is considered as a cold zone (T_C), while the segment of the bottom wall considered as heated zone (T_H). The remaining sections of each wall are assumed to be insulated.

2.1 Governing equations

A two-dimensional steady, incompressible, Newtonian fluid for the study of NC flow inside a triangular porous cavity consisting of two cold static circular cylinders (Bejan, 2013):

$$\frac{\partial U}{\partial X}+\frac{\partial V}{\partial Y}=0 \tag{1}$$

$$U\frac{\partial U}{\partial X}+V\frac{\partial U}{\partial Y}=-\frac{\partial P}{\partial X}+Pr\left(\frac{\partial^2 U}{\partial X^2}+\frac{\partial^2 U}{\partial Y^2}\right)-\frac{Pr}{Da}U \tag{2}$$

$$U\frac{\partial V}{\partial X}+V\frac{\partial V}{\partial Y}=-\frac{\partial P}{\partial Y}+Pr\left(\frac{\partial^2 V}{\partial X^2}+\frac{\partial^2 V}{\partial Y^2}\right)-\frac{Pr}{Da}V+Ra\,\mathrm{Pr}\,\theta \tag{3}$$

$$U\frac{\partial \theta}{\partial X}+V\frac{\partial \theta}{\partial Y}=\left(\frac{\partial^2 \theta}{\partial X^2}+\frac{\partial^2 \theta}{\partial Y^2}\right) \tag{4}$$

where

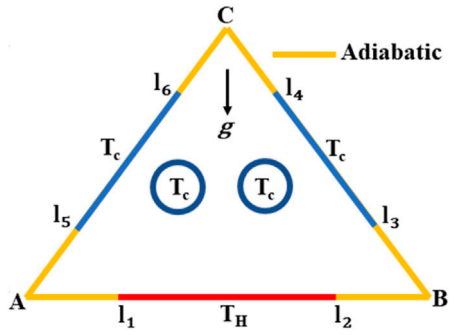

FIGURE 1
Physical diagram of an equilateral triangular cavity.

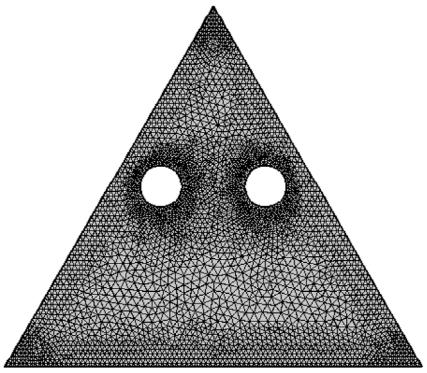

FIGURE 2
Mesh elements of the triangular cavity.

$$X = \frac{x}{L}, Y = \frac{y}{L}, U = \frac{uL}{\alpha}, V = \frac{vL}{\alpha}, \theta = \frac{T - T_C}{T_H - T_C}, P = \frac{pL^2}{\rho\alpha^2},$$
$$Pr = \frac{\nu}{\alpha}, Da = \frac{K}{L^2}, Ra = \frac{g\beta(T_H - T_C)L^3\, Pr}{\nu^2} \quad (5)$$

Here, X and Y are considered non-dimensional Cartesian coordinates system, and U and V are correspondingly non-dimensional velocity components. Moreover, θ is the non-dimensional temperature and P is the non-dimensional pressure.

2.2 Boundary conditions

The research investigates the no-slip boundary condition within fluid dynamics, a foundational principle dictating that fluid motion is stopped at solid boundaries within a triangular cavity. Both fluid velocity and temperature boundary conditions are pivotal aspects examined in the study. The outlined boundary conditions for fluid velocity and temperature are provided below:

$$U(X,0) = V(X,0) = 0 \text{ on } AB,$$
$$U(X,Y) = V(X,Y) = 0 \text{ on } AC \text{ and } U(X,Y) = 0 \text{ on } BC \quad (6)$$
$$T = T_H \text{ on } l_1l_2, T = T_C \text{ on } l_3l_4 \text{ and } l_5l_6 \quad (7)$$

In the study, the length of the heated bottom wall (l_1l_2) of triangular cavity is denoted by ε, see Figure 1. The numerical experiments conducted in the study involve varying this parameter, with values ranging from 0.2 to 0.8.

2.2.1 Non-dimensional parameters

2.2.1.1 *Nusselt number* (Saha et al., 2010)

The average Nusselt number (Nu_{avg}) of the hot bottom wall of the triangular cavity is expressed as:

$$Nu_{avg} = \overline{Nu} = -\frac{1}{\varepsilon}\int_{X=0}^{\varepsilon}\left(\frac{\partial\theta}{\partial Y}\right)dX \quad (8)$$

Entropy generation due to heat transfer (Ilis et al., 2008):

$$E_{HT} = \left(\frac{\partial\theta}{\partial X}\right)^2 + \left(\frac{\partial\theta}{\partial Y}\right)^2 \quad (9)$$

Entropy generation due to fluid friction (Ilis et al., 2008):

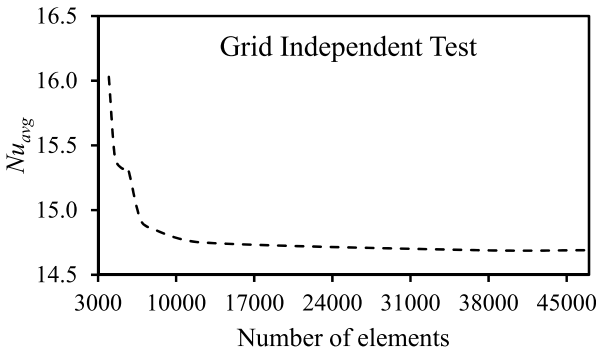

FIGURE 3
Grid Independent test results.

$$E_{FF} = \phi\left[(U^2 + V^2) + Da\left\{2\left(\left(\frac{\partial\theta}{\partial X}\right)^2 + \left(\frac{\partial\theta}{\partial Y}\right)^2\right) + \left(\frac{\partial U}{\partial X} + \frac{\partial V}{\partial Y}\right)^2\right\}\right] \quad (10)$$

where, $\phi = 10^{-4}$ is the irreversibility distribution ratio.

2.2.1.2 *Total Entropy generation* (Ilis et al., 2008)

$$E_{gen} = E_{HT} + E_{FF} \quad (11)$$

Bejan number (Ilis et al., 2008):

$$Be = \frac{E_{HT}}{E_{gen}} \quad (12)$$

3 Numerical method, grid independent test and validation

A numerical approach is employed to investigate natural convection (NC) within a porous triangular cavity containing two stationary circular cylinders. The commercial software COMSOL Multiphysics is utilized to solve Eqs 1–7 using Finite

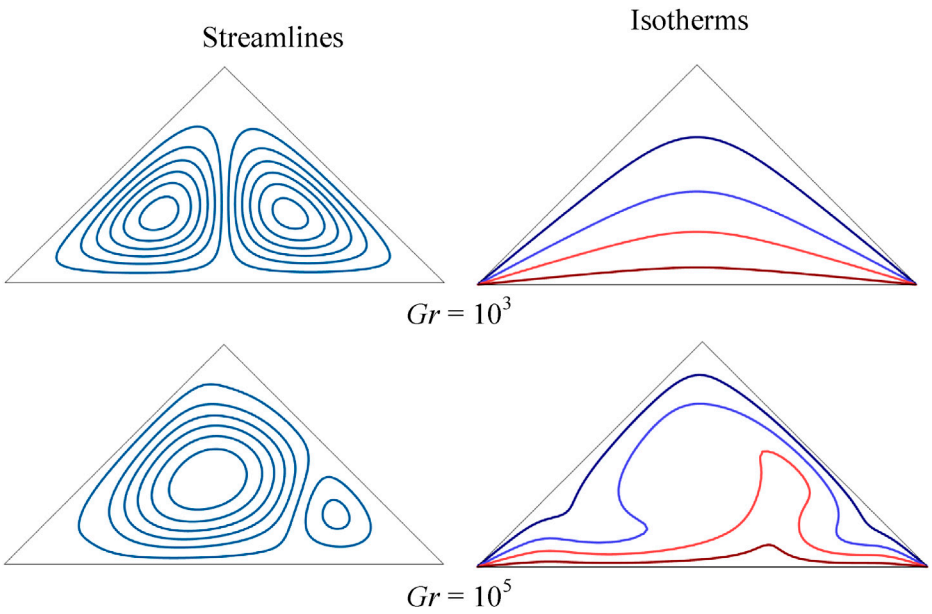

FIGURE 4
Results of streamlines and isotherms of our study for Gr = 10^3 and 10^5.

Element Method (FEM), and simulations are conducted for air. A very fine triangular mesh was applied along the hot and cold walls and around the cold cylinders to calculate the sharp changes in temperature and velocity, as shown in Figure 2. A stationary linear direct solver, PARDISO, was used to solve the equations generated by FEM. PARDISO solver is preferred for a small number of degrees of freedom because it is more stable and faster, although it consumes memory at a high rate. The relative tolerance for the convergence criterion was set to 10^{-6}.

3.1 Grid independent test

We know the grid independent test confirms the accuracy of numerical simulations, ensuring that outcomes converge to consistent solutions regardless of grid refinement. As depicted in Figure 3, the test is performed for Nu_{avg} with different grid sizes ranging from 3,000 to 48,000. Analysis of Figure 3 reveals that the variation in Nu_{avg} is insignificant when transitioning from 38,000 to 45,000 mesh elements. Hence, 38,000 mesh elements are selected as the optimal mesh size for our study.

3.2 Validation

Figure 4 presents streamlines and isotherms within a triangular cavity at Gr of 10^3 and 10^5, showing the present findings. Our study's results demonstrate a notable agreement with Holtzman et al.'s findings. Additionally, validation was conducted by comparing Nu_{avg} across various Gr values, as detailed in Table 1. The comparison reveals closely aligned values between our findings and those of Holtzman et al. (Holtzman et al., 2000).

4 Results

The current numerical simulation explores the fluid flow and HT dynamics within a porous triangular cavity filled with air. Various parameters are analyzed, including ε (0.1–0.9), as well as the impact of varying Ra (10^3–10^6), Pr (0.71), and Da (10^{-5} to 10^{-2}) numbers. Also, results related to Eqs 8–12 are presented qualitatively and quantitatively in this section.

4.1 Variation of ra

Figure 5 shows the variation of streamlines, isotherms, E_{FF}, E_{HT}, and Be for different Ra. As we know, higher Ra values indicate the dominant role of convection over conduction in HT. So, the streamline plots exhibit an upward trend with the increase of Ra. Two counter-rotating cellular flows below the cold domain but adjacent to the lower hot wall are prominent in all the cases. Flow patterns are found symmetrical throughout the ranges of the Ra. Isotherms also demonstrate similar upward trends with the rise of Ra with the temperature distribution from the lower hot wall towards both the cold side walls. Increasing buoyant forces with higher Ra makes the fluid flow stronger, and the isotherms shift away from the sidewalls to the center. Hence, relatively hot fluid will pass along the cavity's centreline and rise between the stationary cold cylinders, demonstrating a plume shape in the isotherms at higher Ra. Moreover, E_{FF} and E_{HT} indicate the irreversibility created in the system. The E_{FF} due to the viscous forces present in the fluid is of much lower value than the E_{HT} due to the presence of a finite temperature gradient. Also, Figure 5 shows a more uniform pattern for E_{HT} as compared to E_{FF} across the Ra. In addition, Be contours in Figure 5 show the share of HT in the total irreversibility. At lower Ra, local Be is found higher in the narrow contrivances (*viz.* Between the stationary cylinder and the sidewalls) due to a higher velocity gradient. However, with the increase of buoyant force due to the rise of Ra, the

TABLE 1 Comparison of the present Nu_{avg} values with Holtzman et al. (Holtzman et al., 2000).

	A = 1.0 and Nu_{avg}		
	$Gr = 10^3$	$Gr = 10^4$	$Gr = 10^5$
Holtzman et al. (2000)	1.00	1.07	1.80
Present results	1.00	1.09	1.90

share of HT in the total irreversibility is increased, and hence, higher local *Be* occupied further areas in the attic.

4.2 Variation of Da

Figure 6 shows the results of various *Da* on the E_{FF} and E_{TH} contours and *Be* plots with $Ra = 10^6$, $\varepsilon = 0.8$, and Pr = 0.71. Higher *Da* indicates a higher permeability. Hence, more hot fluid will flow through the pores and thus increasing the convection. Hence, the density of E_{FF} and E_{TH} contours are increased, especially near the enclosures as evident in Figure 5. The local *Be* contours indicate isentropic spots near the cold pipe walls at lower *Da* values. However, these spots have become wider and denser with the rise of permeability levels aiding HT. However, symmetrical patterns are observed across the *Da* values.

4.3 Variation of ε

Figure 7 represents the results of various lengths of heat source *(ε)* on the streamlines, isotherms, E_{FF} and E_{TH} contours and *Be* plots for different ε with $Ra = 10^6$, $Da = 10^{-2}$, and Pr = 0.71. At a small ε value of 0.2, the cavity exhibits a flow characterized by two streamlined rotating cells: one featuring counterclockwise

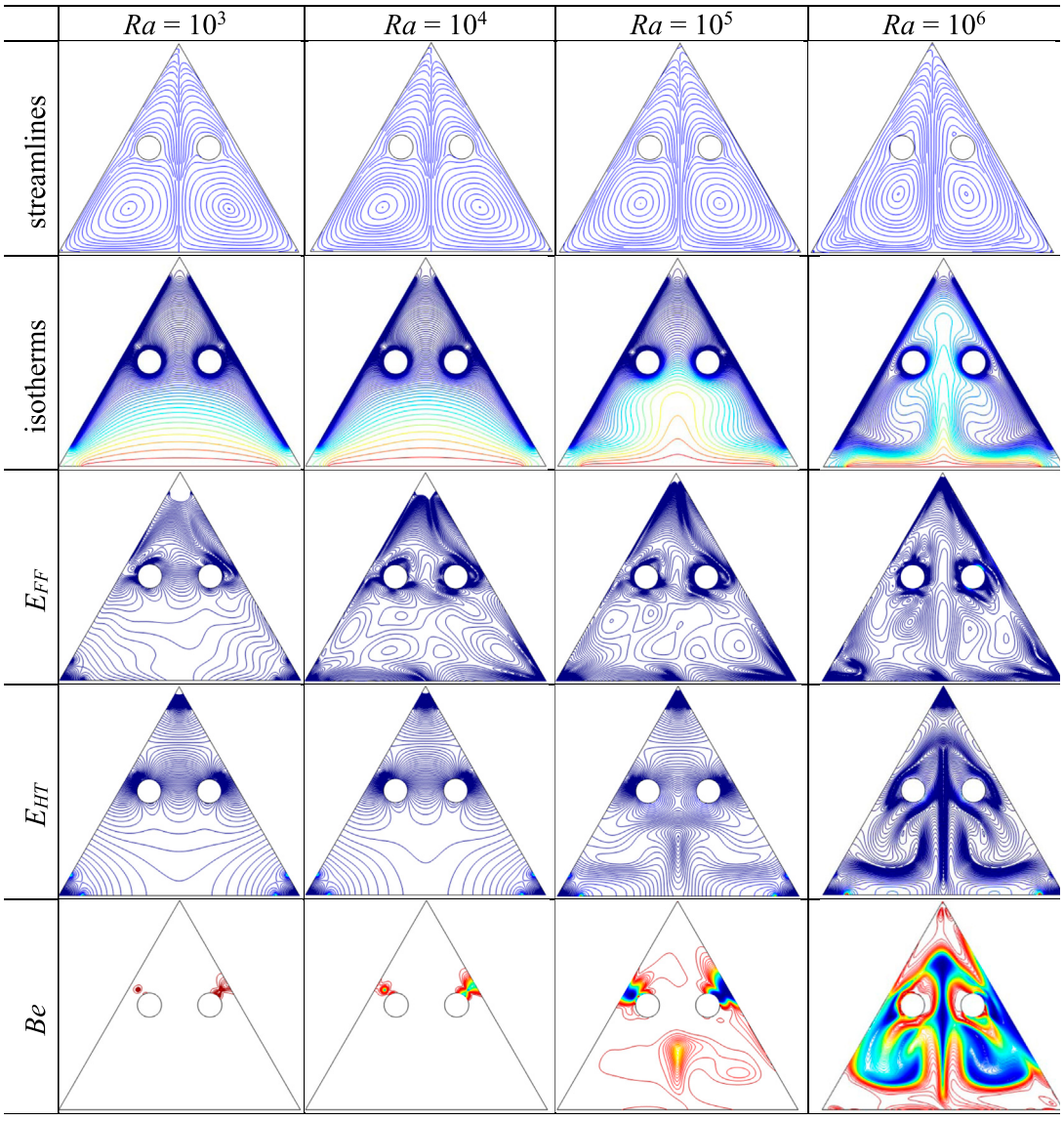

FIGURE 5
Variation of streamlines, isotherms, E_{FF}, E_{HT}, and *Be* for different *Ra* with $Da = 10^{-2}$, and $\varepsilon = 0.8$.

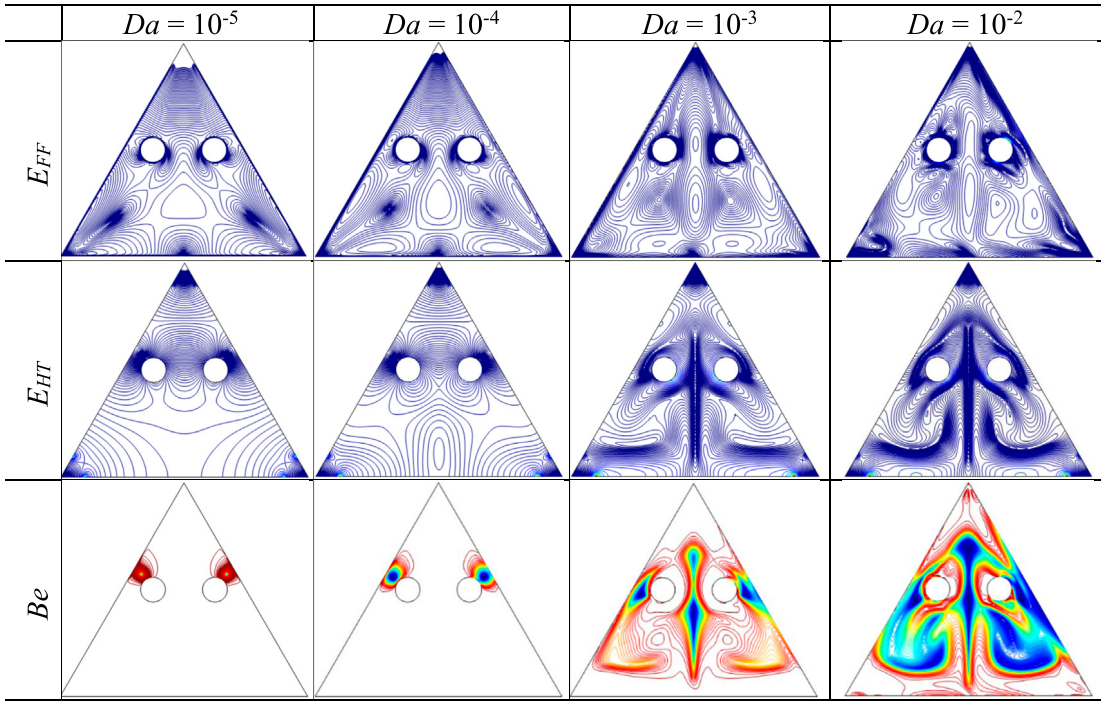

FIGURE 6
Variation of E_{FF}, E_{HT}, and Be for different Da with Ra = 10^6, and ε = 0.8.

fluid heat flow on the left and the other showcasing clockwise fluid heat flow on the right. The isotherms display curved trajectories originating from the cold stationary sources, with intense isotherms gathering near the bottom wall, indicative of the presence of the hot source. Also, isentropic patterns apparent as stretched spot shapes proximal to the walls. It is observe that increasing ε value notably alters flow dynamics and temperature distribution. Figure 7 also reveals that an increase in the length of the hot wall *(ε)* significantly reduces the HT rate, as indicated by the isotherm plot and Nu furnished in Table 2. Additionally, E_{FF}, and E_{HT} increases with the elongation of ε, while *Be* consistently rises with the extension of ε within the triangular cavity, especially near the cylinder surfaces and at the cavity walls. Flow features indicated by streamlines exhibit a steady and symmetric pattern throughout the variation of ε. A small corner vortices are noticed at a lower value of ε, however the same disappears at higher ε.

4.4 Variation of Nu_{avg}

Table 2 describes the influence of parameters such as ε, *Ra*, and *Da* on HT efficiency within a fluid system. Notably, an increase in ε from 0.2 to 0.4 leads to a significant decrease in the Nu_{avg}, indicating reduced HT effectiveness. Further increments in ε to 0.6 and 0.8 result in diminishing changes in Nu_{avg}, suggesting that beyond ε = 0.4, the decline in HT becomes less pronounced. Additionally, at $Ra = 10^4$, Nu_{avg} decreases with increasing *Ra* for varying ε values, implying less efficient HT at lower *Ra* values. However, for $Ra = 10^5$ and 10^6, Nu_{avg} increases, indicating improved HT efficiency at higher *Ra* values.

4.5 Variation of E_{gen}

Table 3 describes the influence of parameters such as ε, *Ra*, and *Da* on E_{gen}. Especially, increasing ε leads to a corresponding rise in E_{gen} for specific values of *Ra*, suggesting an escalation in irreversibility and entropy production within the system. Likewise, as *Ra* increases from 10^3 to 10^6 for a fixed ε, E_{gen} also increases, signifying heightened irreversibility and entropy production at higher *Ra* values. Furthermore, an increase in ε for different values of *Da* and *Ra* (=10^6) results in a proportional increase in E_{gen}, indicating a direct link between higher ε values and increased entropy production. Similarly, for constant ε values, as *Da* rises from 10^{-5} to 10^{-2}, E_{gen} also intensifies, highlighting the contribution of higher *Da* values to greater entropy production in the system.

4.6 Variation of Be

Table 4 describes the influence of parameters such as ε, *Ra*, and *Da* on *Be*. The dynamics of *Be* concerning variations in ε and *Da* reveal interesting patterns. When $Da = 10^{-5}$, augmenting ε leads to a decline in *Be*, suggesting that higher ε values correspond to improved HT efficiency and diminished irreversibility. Conversely, at $Da = 10^{-4}$, elevating ε from

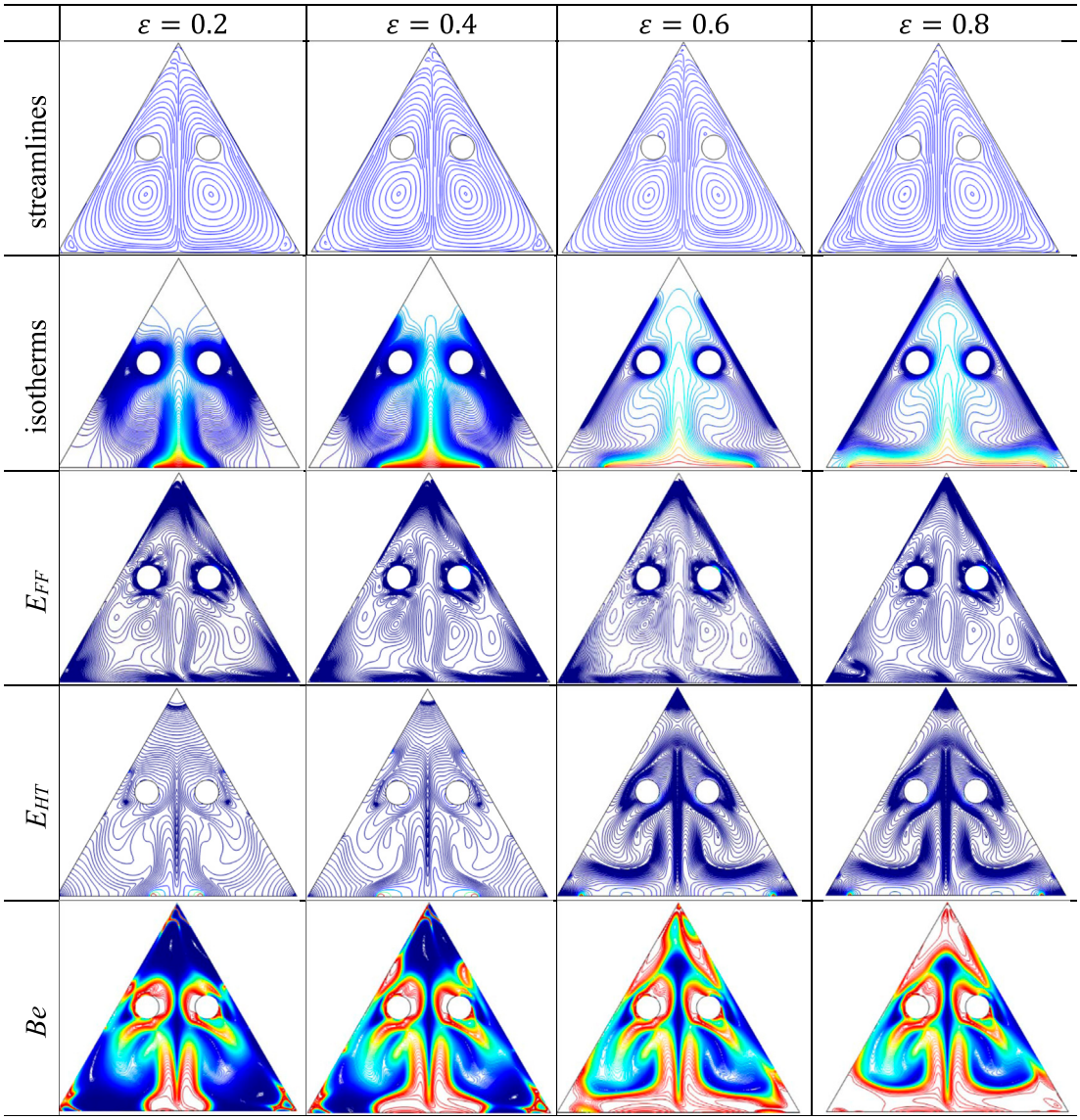

FIGURE 7
Variation of streamlines, isotherms, E_{FF}, E_{HT}, and *Be* for different ε with $Ra = 10^6$, and $Da = 10^{-2}$.

0.2 to 0.4 initially results in a decrease in *Be*, indicating enhanced HT efficiency, but further increments to 0.6 and 0.8 cause *Be* to rise, implying a shifting equilibrium between HT and irreversibility. For $Da = 10^{-3}$ and 10^{-2}, increasing ε results in a higher *Be*, indicating a greater presence of irreversibility in the system. Moreover, maintaining a constant ε value while increasing *Da* correlates with a decrease in *Be*, potentially reflecting improved HT efficiency and reduced irreversibility for higher *Da* values under specific ε conditions.

5 Discussions

The numerical simulations conducted in this study reveal significant insights into the behaviour of NC and E_{gen} within a porous triangular cavity containing two cold circular cylinders. The variations in *Ra*, *Da*, and ε demonstrate complex interactions between fluid dynamics and HT.

5.1 Impact of *Ra*

The increase in *Ra* from 10^3 to 10^6 enhances the buoyancy-driven convective flow, as evidenced by the upward trends in the streamline and isotherm plots (Figure 5). Higher *Ra* values indicate a dominant convective HT mechanism over conduction. This is reflected in the formation of plume-shaped isotherms at higher *Ra*, signifying stronger fluid motion and more efficient heat transport away from the heated wall. The enhanced convective flow also leads to increased E_{gen} due to both HT and FF, with E_{gen} due to both HT being more prominent. These results align with the fundamental principles of thermodynamics, where increased

10.3389/fenrg.2024.1422256

TABLE 2 *Variation of* Nu_{avg} for different ε, *Ra*, and *Da*

Parameters		$\varepsilon = 0.2$	$\varepsilon = 0.4$	$\varepsilon = 0.6$	$\varepsilon = 0.8$
$Da = 10^{-2}$	$Ra = 10^3$	20.218	8.289	6.5457	5.4892
	$Ra = 10^4$	19.797	8.045	6.5431	5.4895
	$Ra = 10^5$	26.919	13.379	11.609	8.2709
	$Ra = 10^6$	54.743	31.129	25.315	14.878
$Ra = 10^6$	$Da = 10^{-5}$	19.87	8.1318	6.5222	5.4678
	$Da = 10^{-4}$	8.1318	8.4713	8.3548	6.2286
	$Da = 10^{-3}$	47.926	26.467	21.427	13.287
	$Da = 10^{-2}$	54.743	31.129	25.315	14.878

TABLE 3 *Variation of* E_{gen} *for different Da and Ra.*

Parameters		$\varepsilon = 0.2$	$\varepsilon = 0.4$	$\varepsilon = 0.6$	$\varepsilon = 0.8$
$Da = 10^{-2}$	$Ra = 10^3$	2.8615	4.2242	6.1193	9.3227
	$Ra = 10^4$	2.8697	4.2545	6.1440	9.3447
	$Ra = 10^5$	5.0571	8.5267	11.106	13.906
	$Ra = 10^6$	12.399	21.379	27.656	28.096
$Ra = 10^6$	$Da = 10^{-5}$	2.8636	4.2391	6.1268	9.3296
	$Da = 10^{-4}$	3.6678	6.1258	8.1408	10.816
	$Da = 10^{-3}$	9.7715	16.625	20.7	22.49
	$Da = 10^{-2}$	12.399	21.379	27.656	28.096

thermal gradients and fluid velocities contribute to higher entropy production.

5.2 Impact of *Da*

Variations in *Da* from 10^{-5} to 10^{-2} indicate changes in the permeability of the porous medium, significantly affecting the fluid flow and HT. Higher *Da* values allow more hot fluid to pass through the pores, increasing convective HT and E_{gen}, particularly near the cavity walls (Figure 6). The local *Be* contours reveal isentropic spots near the cold pipe walls at lower *Da* values, which become denser with higher permeability, aiding HT. The symmetrical patterns observed across different *Da* values suggest a consistent influence of permeability on the system's thermal behaviour.

5.3 Impact of ε

Increasing the length of the heated segment (ε) from 0.2 to 0.8 results in notable changes in flow dynamics and temperature distribution (Figure 7). A smaller ε value (0.2) exhibits two distinct rotating cells, while larger ε values reduce the HT rate, as indicated by the isotherm plots and Nu_{avg} values in Table 2. This reduction is due to the increased area over which heat must be dissipated, leading to lower temperature gradients and less efficient HT. Additionally, both E_{gen} due to FF and HT increase with larger ε values, highlighting the role of heated segment length in enhancing E_{gen} within the cavity.

TABLE 4 *Variation of Be* for different *Da* and *Ra*.

		$\varepsilon = 0.2$	$\varepsilon = 0.4$	$\varepsilon = 0.6$	$\varepsilon = 0.8$
$Da = 10^{-2}$	$Ra = 10^3$	0.99999	0.99995	0.99992	0.99992
	$Ra = 10^4$	0.99873	0.99609	0.99512	0.99508
	$Ra = 10^5$	0.87358	0.92253	0.94436	0.94639
	$Ra = 10^6$	0.3316	0.4146	0.56913	0.62436
$Ra = 10^6$	$Da = 10^{-5}$	0.99979	0.99918	0.99887	0.99885
	$Da = 10^{-4}$	0.98059	0.97800	0.97991	0.98049
	$Da = 10^{-3}$	0.62617	0.72729	0.84351	0.86788
	$Da = 10^{-2}$	0.3316	0.41460	0.56913	0.62436

6 Practical implications

The findings from this study have practical implications for the design of eco-friendly cooling systems, particularly in buildings located in hot climates. By optimizing the parameters studied (*Ra*, *Da*, and ε), engineers can design more efficient passive cooling systems that reduce energy consumption and mitigate urban heat island effects. The insights gained from E_{gen} analysis can inform the development of advanced HT systems, such as heat exchangers and electronic cooling devices, where minimizing entropy production is crucial for enhancing performance and efficiency.

7 Conclusion

Our detailed study investigated how physical factors interact in a porous triangular space with two cylinders. We focused on understanding HT, fluid dynamics, and E_{gen} for air. By analyzing *Ra*, *Da*, and ε, we observed changes in the system. Some important findings are presented below:

- At strong convection $Ra = 10^6$, the increase in *Da* from the value of $Da = 10^{-5}$ to $Da = 10^{-2}$ led to a sharp rise in HT regardless of the size of the heated segment ε.
- Increasing the active length ε always reduces the average HT rate.
- The rate of E_{gen} always rises with the length of heated segment ε, convection strength *Ra* and the permeability of the airflow within the pores.
- Increasing the convection strength leads to the dominant feature, the viscous irreversibility, over HT irreversibility.
- Increasing the airflow through the pores leads to more convective HT and viscous irreversibility.

Future research could explore experimental validation of the numerical results and investigate the impact of different fluid types and boundary conditions on NC and E_{gen} within porous cavities. Additionally, studies could examine the transient behaviour of the system to understand the time-dependent dynamics of HT and fluid flow.

Data availability statement

The original contributions presented in the study are included in the article/Supplementary Material, further inquiries can be directed to the corresponding author.

Author contributions

AA-W: Formal Analysis, Investigation, Methodology, Visualization, Writing–original draft. ST: Formal Analysis, Investigation, Methodology, Writing–original draft. PN: Investigation, Methodology, Writing–review and editing. AP: Supervision, Writing–original draft, Writing–review and editing. GS: Conceptualization, Project administration, Supervision, Writing–review and editing. SS: Project administration, Resources, Supervision, Writing–review and editing.

Funding

The author(s) declare that no financial support was received for the research, authorship, and/or publication of this article.

Conflict of interest

The authors declare that the research was conducted in the absence of any commercial or financial relationships that could be construed as a potential conflict of interest.

References

Afrand, M., Pordanjani, A. H., Aghakhani, S., Oztop, H. F., and Abu-Hamdeh, N. (2020). Free convection and entropy generation of a nanofluid in a tilted triangular cavity exposed to a magnetic field with sinusoidal wall temperature distribution considering radiation effects. *Int. Commun. Heat Mass Transf.* 112, 104507. doi:10.1016/j.icheatmasstransfer.2020.104507

Amidu, M. A., Addad, Y., Riahi, M. K., and Abu-Nada, E. (2021). Numerical investigation of nanoparticles slip mechanisms impact on the natural convection heat transfer characteristics of nanofluids in an enclosure. *Sci. Rep.* 11 (1), 15678. doi:10.1038/s41598-021-95269-z

Basak, T., Gunda, P., and Anandalakshmi, R. (2012). Analysis of entropy generation during natural convection in porous right-angled triangular cavities with various thermal boundary conditions. *IndraStra Glob.* 55 (17–18), 4521–4535. doi:10.1016/j.ijheatmasstransfer.2012.03.061

Basak, T., Roy, S., Ramakrishna, D., and Pandey, B. D. (2010). Analysis of heat recovery and heat transfer within entrapped porous triangular cavities via heatline approach. *Int. J. Heat Mass Transf.* 53 (19), 3655–3669. doi:10.1016/j.ijheatmasstransfer.2010.03.040

Bejan, A. (2013). Convection heat transfer. *Wiley*. doi:10.1002/9781118671627

Bhardwaj, S., and Dalal, A. (2013). Analysis of natural convection heat transfer and entropy generation inside porous right-angled triangular enclosure. *Int. J. Heat Mass Transf.* 65, 500–513. doi:10.1016/j.ijheatmasstransfer.2013.06.020

Bhardwaj, S., Dalal, A., and Pati, S. (2015). Influence of wavy wall and non-uniform heating on natural convection heat transfer and entropy generation inside porous complex enclosure. *Energy (Oxford)* 79 (C), 467–481. doi:10.1016/j.energy.2014.11.036

Bhowmick, S., Saha, S. C., Qiao, M., and Xu, F. (2019). Transition to a chaotic flow in a V-shaped triangular cavity heated from below. *Int. J. Heat Mass Transf.* 128, 76–86. doi:10.1016/j.ijheatmasstransfer.2018.08.126

Bhowmick, S., Xu, F., Zhang, X., and Saha, S. C. (2018). Natural convection and heat transfer in a valley shaped cavity filled with initially stratified water. *Int. J. Therm. Sci.* 128, 59–69. doi:10.1016/j.ijthermalsci.2018.02.019

Bilal, S., Mahmood, R., Majeed, A. H., Khan, I., and Nisar, K. S. (2020). Finite element method visualization about heat transfer analysis of Newtonian material in triangular cavity with square cylinder. *J. Mater. Res. Technol.* 9 (3), 4904–4918. doi:10.1016/j.jmrt.2020.03.010

Billah, M. M., Rahman, M. M., Razzak, M. A., Saidur, R., and Mekhilef, S. (2013). Unsteady buoyancy-driven heat transfer enhancement of nanofluids in an inclined triangular enclosure. *Int. Commun. Heat Mass Transf.* 49, 115–127. doi:10.1016/j.icheatmasstransfer.2013.09.006

Chamkha, A. J., Selimefendigil, F., and Oztop, H. F. (2018). MHD mixed convection and entropy generation in a lid-driven triangular cavity for various electrical conductivity models. *Entropy Basel, Switz.* 20 (12), 903. doi:10.3390/e20120903

Chatterjee, D., Manna, N. K., and Biswas, N. (2022). Thermo-magnetic convection of nanofluid in a triangular cavity with a heated inverted triangular object. *Mater. Today Proc.* 52, 427–433. doi:10.1016/j.matpr.2021.09.093

Chen, C.-L., and Cheng, C.-H. (2009). Numerical study of the effects of lid oscillation on the periodic flow pattern and convection heat transfer in a triangular cavity. *Int. Commun. Heat Mass Transf.* 36 (6), 590–596. doi:10.1016/j.icheatmasstransfer.2009.03.006

Ching, Y. C., Öztop, H. F., Rahman, M. M., Islam, M. R., and Ahsan, A. (2012). Finite element simulation of mixed convection heat and mass transfer in a right triangular enclosure. *Int. Commun. Heat Mass Transf.* 39 (5), 689–696. doi:10.1016/j.icheatmasstransfer.2012.03.016

Das, D., Lukose, L., and Basak, T. (2017). Role of finite element based grids and simulations on evaluation of Nusselt numbers for heat functions within square and triangular cavities involving multiple discrete heaters. *Int. Commun. Heat Mass Transf.* 89, 39–46. doi:10.1016/j.icheatmasstransfer.2017.09.008

Fayz-Al-Asad, M., Nur Alam, M., Ahmad, H., Sarker, M. M. A., Alsulami, M. D., and Gepreel, K. A. (2021). Impact of a closed space rectangular heat source on natural convective flow through triangular cavity. *Results Phys.* 23, 104011. doi:10.1016/j.rinp.2021.104011

Hasanuzzaman, M., Rahman, M. M., Öztop, H. F., Rahim, N. A., and Saidur, R. (2012). Effects of Lewis number on heat and mass transfer in a triangular cavity. *Int. Commun. Heat Mass Transf.* 39 (8), 1213–1219. doi:10.1016/j.icheatmasstransfer.2012.07.002

Holtzman, G. A., Hill, R. W., and Ball, K. S. (2000). Laminar natural convection in isosceles triangular enclosures heated from below and symmetrically cooled from above. *J. Heat Transf.* 122 (3), 485–491. doi:10.1115/1.1288707

Ikram, M. M., Saha, G., and Saha, S. C. (2021). Conjugate forced convection transient flow and heat transfer analysis in a hexagonal, partitioned, air filled cavity with dynamic modulator. *Int. J. Heat Mass Transf.* 167, 120786. doi:10.1016/j.ijheatmasstransfer.2020.120786

Ikram, M. M., Saha, G., and Saha, S. C. (2023). Unsteady conjugate heat transfer characteristics in hexagonal cavity equipped with a multi-blade dynamic modulator. *Int. J. Heat Mass Transf.* 200, 123527. doi:10.1016/j.ijheatmasstransfer.2022.123527

Ikram, M. M., Saha, G., and Saha, S. C. (2024). Second law analysis of a transient hexagonal cavity with a rotating modulator. *Int. J. Heat Mass Transf.* 221, 125039. doi:10.1016/j.ijheatmasstransfer.2023.125039

Ilis, G. G., Mobedi, M., and Sunden, B. (2008). Effect of aspect ratio on entropy generation in a rectangular cavity with differentially heated vertical walls. *Int. Commun. Heat Mass Transf.* 35 (6), 696–703. doi:10.1016/j.icheatmasstransfer.2008.02.002

Kumar, C., Chatterjee, D., and Mondal, B. (2021). The role of cross thermal buoyancy in initiating vortex shedding behind a permeable square cylinder at low Reynolds numbers. *J. Porous Media* 24 (11), 65–84. doi:10.1615/JPorMedia.2021036458

Kumar, C., Chatterjee, D., and Mondal, B. (2023). Effect of porosity and transverse magnetic field on the wake separation and detachment around a porous square cylinder. *Transp. Porous Media* 146 (3), 805–825. doi:10.1007/s11242-022-01889-y

Li, B., Xu, H., Song, Y.-J., Zhang, H.-L., Wang, W.-W., and Zhao, F.-Y. (2023). Heat and moisture transports in a slot ventilated enclosure packed with discrete porous

media: mixing convection instability, oscillation and resonance. *Int. J. Therm. Sci.* 194, 108603. doi:10.1016/j.ijthermalsci.2023.108603

Li, Z., Shahsavar, A., Niazi, K., Al-Rashed, A. A. A. A., and Talebizadehsardari, P. (2020). The effects of vertical and horizontal sources on heat transfer and entropy generation in an inclined triangular enclosure filled with non-Newtonian fluid and subjected to magnetic field. *Powder Technol.* 364, 924–942. doi:10.1016/j.powtec.2019.10.076

Liu, W., Shahsavar, A., Barzinjy, A. A., Al-Rashed, A. A. A. A., and Afrand, M. (2019). Natural convection and entropy generation of a nanofluid in two connected inclined triangular enclosures under magnetic field effects. *Int. Commun. Heat Mass Transf.* 108, 104309. doi:10.1016/j.icheatmasstransfer.2019.104309

Mansouri, A., Binali, A., Aljawi, A., Alhammadi, A., Almir, K., Alnuaimi, E., et al. (2022). Thermal modeling of the convective heat transfer in the large air cavities of the 3D concrete printed walls. *Cogent Eng.* 9 (1). doi:10.1080/23311916.2022.2130203

Nag, S., Sen, N., Bamboowala, H. T., Manna, N. K., Biswas, N., and Mandal, D. K. (2022). MHD nanofluid heat transport in a corner-heated triangular enclosure at different inclinations. *Mater. TODAY-PROCEEDINGS* 63, 141–148. doi:10.1016/j.matpr.2022.02.421

Rahman, M. M., Alam, M. S., Al-Salti, N., and Eltayeb, I. A. (2016). Hydromagnetic natural convective heat transfer flow in an isosceles triangular cavity filled with nanofluid using two-component nonhomogeneous model. *Int. J. Therm. Sci.* 107, 272–288. doi:10.1016/j.ijthermalsci.2016.04.009

Rahman, M. M., Billah, M. M., Rahman, A. T. M. M., Kalam, M. A., and Ahsan, A. (2011). Numerical investigation of heat transfer enhancement of nanofluids in an inclined lid-driven triangular enclosure. *Int. Commun. Heat Mass Transf.* 38 (10), 1360–1367. doi:10.1016/j.icheatmasstransfer.2011.08.011

Rahman, M. M., Öztop, H. F., Ahsan, A., and Orfi, J. (2012). Natural convection effects on heat and mass transfer in a curvilinear triangular cavity. *Int. J. Heat Mass Transf.* 55 (21–22), 6250–6259. doi:10.1016/j.ijheatmasstransfer.2012.06.055

Riahi, M. K., Ali, M., Addad, Y., and Abu-Nada, E. (2022). Combined Newton–Raphson and Streamlines-Upwind Petrov–Galerkin iterations for nanoparticles transport in buoyancy-driven flow. *J. Eng. Math.* 132 (1), 22. doi:10.1007/s10665-021-10205-4

Saboj, J. H., Nag, P., Saha, G., and Saha, S. C. (2023). Entropy production analysis in an octagonal cavity with an inner cold cylinder: a thermodynamic aspect. *Energies (Basel)* 16 (14), 5487. doi:10.3390/en16145487

Saboj, J. H., Nag, P., Saha, G., and Saha, S. C. (2024). Heat transfer assessment incorporated with entropy generation within a curved corner structure enclosing a cold domain. *Heat. Transf.* 53, 2460–2479. doi:10.1002/htj.23044

Saha, B. K., Jihan, J. I., Ahammad, Md. Z., Saha, G., and Saha, S. C. (2024a). Enhanced thermal performance and entropy generation analysis in a novel cavity design with circular cylinder. *Heat. Transf.* 53, 1446–1473. doi:10.1002/htj.22999

Saha, G., Al-Waaly, A. A. Y., Ikram, M. M., Bihani, R., and Saha, S. C. (2024b). Unveiling the dynamics of entropy generation in enclosures: a systematic review. *Int. J. Thermofluids* 21, 100568. doi:10.1016/j.ijft.2024.100568

Saha, G., Al-Waaly, A. A. Y., Paul, M. C., and Saha, S. C. (2023). Heat transfer in cavities: configurative systematic review. *Energies (Basel)* 16 (5), 2338. doi:10.3390/en16052338

Saha, G., Saha, S., Hasan, M. N., and Islam, M. Q. (2010). Natural convection heat transfer within octagonal enclosure. *Int. J. Eng. Trans. A Basics* 23 (1), 1–10.

Saha, T., Saha, G., Parveen, N., and Islam, T. (2024c). Unsteady magneto-hydrodynamic behavior of TiO2-kerosene nanofluid flow in wavy octagonal cavity. *Int. J. Thermofluids* 21, 100530. doi:10.1016/j.ijft.2023.100530

Selimefendigil, F., and Öztop, H. F. (2016). Natural convection in a flexible sided triangular cavity with internal heat generation under the effect of inclined magnetic field. *J. Magnetism Magnetic Mater.* 417, 327–337. doi:10.1016/j.jmmm.2016.05.053

Selimefendigil, F., and Öztop, H. F. (2017). Mixed convection in a partially heated triangular cavity filled with nanofluid having a partially flexible wall and internal heat generation. *J. Taiwan Inst. Chem. Eng.* 70, 168–178. doi:10.1016/j.jtice.2016.10.038

Sharif, M. A. R., and Mohammad, T. R. (2005). Natural convection in cavities with constant flux heating at the bottom wall and isothermal cooling from the sidewalls. *Int. J. Therm. Sci.* 44 (9), 865–878. doi:10.1016/j.ijthermalsci.2005.02.006

Shekaramiz, M., Fathi, S., Ataabadi, H. A., Kazemi-Varnamkhasti, H., and Toghraie, D. (2021). MHD nanofluid free convection inside the wavy triangular cavity considering periodic temperature boundary condition and velocity slip mechanisms. *Int. J. Therm. Sci.* 170, 107179. doi:10.1016/j.ijthermalsci.2021.107179

Sheremet, M. A., Grosan, T., and Pop, I. (2017). Natural convection and entropy generation in a square cavity with variable temperature side walls filled with a nanofluid: buongiorno's mathematical model. *Entropy Basel, Switz.* 19 (7), 337. doi:10.3390/e19070337

Soomro, F. A., Haq, R. U., Algehyne, E. A., and Tlili, I. (2020). Thermal performance due to magnetohydrodynamics mixed convection flow in a triangular cavity with circular obstacle. *J. Energy Storage* 31, 101702. doi:10.1016/j.est.2020.101702

Uddin, M. J., Al-Balushi, J., Mahatabuddin, S., and Rahman, M. M. (2022). Convective heat transport for copper oxide-water nanofluid in an isosceles triangular cavity with a rippled base wall in the presence of magnetic field. *Int. J. Thermofluids* 16, 100195. doi:10.1016/j.ijft.2022.100195

Varol, Y., Oztop, H. F., Mobedi, M., and Pop, I. (2008b). Visualization of natural convection heat transport using heatline method in porous non-isothermally heated triangular cavity. *Int. J. Heat Mass Transf.* 51 (21), 5040–5051. doi:10.1016/j.ijheatmasstransfer.2008.04.023

Varol, Y., Oztop, H. F., and Varol, A. (2008a). Free convection heat transfer and flow field in triangular enclosures filled with porous media. *J. Porous Media* 11 (1), 103–115. doi:10.1615/JPorMedia.v11.i1.70

Nomenclature

A	Aspect ratio
Be	Bejan number
Da	Darcy number
E_{FF}	Entropy generation due to fluid friction
E_{gen}	Entropy generation
E_{HT}	Entropy generation due to heat transfer
F	Fluid friction
Gr	Grashof number
HT	Heat transfer
Ha	Hartman number
L	Triangular side length
Nu	Nusselt number
Nu_{avg}	Average Nusselt number
P	Non-dimensional pressure
Pr	Prandtl number
Ra	Rayleigh number
T_C	Cold temperature
T_H	Hot temperature
U	Non-dimensional velocity component in the horizontal direction
V	Non-dimensional velocity component in the vertical direction
X	Non-dimensional coordinate in the horizontal direction
Y	Non-dimensional coordinate in the vertical direction
Greek symbols	
E	Length of the hot or cold wall
θ	Non-dimensional temperature Subscription
avg	Average
gen	Generation
C	Cold
H	Hot